Phase Behavior, Topology, and Growth of Neutral Catanionic Reverse Micelles

ARTICLE *in* LANGMUIR · OCTOBER 2006

Impact Factor: 4.46 · DOI: 10.1021/la061465r · Source: PubMed

Phase Behavior, Topology, and Growth of Neutral Catanionic Reverse Micelles

Benjamin Abécassis,*,† Fabienne Testard,*,† Lise Arleth,‡ Steen Hansen,‡ Isabelle Grillo,§ and Thomas Zemb†

LIONS − CEA Saclay 9119, Gif-Sur-Yvette, France, Biophysics, Department of Natural Sciences, The Royal Veterinary and Agricultural University, Thorvaldensevej 40, DK-1871 Frederiksberg C, Denmark, and Institut Laue-Langevin, DS/LSS, 6 rue Jules Horowitz, B.P. 156, 38042 Grenoble, France

Received May 24, 2006. In Final Form: July 11, 2006

The ternary catanionic system octylammoniumoctanoate/octane/water is studied by combined SANS, light scattering, conductivity, and phase diagram approach in the water-poor microemulsion region. The sphere-to-cylinder growth and branching depends on the concentration, the water-to-surfactant ratio, and the temperature. The unidimensional growth leads to a network of interconnected wormlike micelles. Like most studied linear nonionic surfactants, in this true catanionic system at equimolarity of anionic and cationic surfactant, the curvature toward water increases with temperature, making connections between cylinders less frequent.

1. Introduction

Catanionic surfactants are mixtures of anionic and cationic surfactants. The term was coined in Lund, when unexpected swelling of uncharged lamellar phases due to the hydration force was under investigation.[1] In water, depending on the composition, catanionic surfactants can self-assemble into original microstructures such as equilibrium vesicles,[2] wormlike micelles,[3] disks,[4] or regular hollow icosahedra[5] which mimics viral capsides and gives new insights into the mode of formation of hollow crystals.[6] In the two last cases, the surfactant is stacked into rigid bilayers where the chains are frozen at ambient temperature. There are two very different subclasses of catanionic mixtures: the first one is the true catanionics when surfactants are mixed in acid and hydroxide form and no salt from the initial counterions is present.[7] In these systems, phase prisms have been established.[8] The second class is when counterions are present. This is the most frequently studied type of catanionic. When the mixed surfactants are in sodium and in bromide form for instance, at least five components are present, and to our knowledge, no equilibrium phase diagram has yet been published. An intermediate case is when one of the counterions is a hydrotrope, i.e., penetrates in the surfactant film, such that only one type of counterion is present in the double layer. The case of tosylate as initial counterion of the cationic moiety of the surfactant pair used has been pioneered by Kaler and co-workers.[9] A few reviews on this growing field of catanionics are available.[8,10,11] In all catanionics systems, the most important parameter is the mole ratio of anionic and cationic surfactant used since it controls the structural surface charge. At equimolarity, there is zero charge and no electrostatic interaction is present as the driving force for swelling. When one of the components is in excess, the structural surface charge of the surfactant film can be chosen in sign and magnitude. The system can be tuned from an uncharged nonionic or zwitterionic system for which curvature (counted positively when directed toward water) increases when temperature increases to an ionic system.

We study here a true catanionics system at equimolar ratio composed of octylammonium-octanoate as surfactant, alkane, and water. In this case, the catanionic surfactant is an equimolar mixture of octylamine and octanoic acid. In true catanionics, the electrostatic is not screened via the excess salt formed by counterions. Due to the electrostatic attraction between the two opposite charges of the ionic heads, catanionic surfactants should share features with double tail zwitterionic surfactants and lipids.[10] Jonsson and co-workers[12] determined the extension of the reverse microemulsion domain in the phase diagram of the octylammonium-octanoate/water/octane system. They showed that the solubilization of water can be greatly increased by mixing a small amount of sodium carboxylate salt to the neutral catanionic surfactant. By NMR experiments, they also showed that the shape of the micelles was certainly not spherical but no further structural characterization has been performed on this system. This observation made our motivation to study the same system with different techniques. Other authors have investigated similar alkylammonium alkanoates/water/oil system to identify the reverse microemulsion domain: heptylammoniumheptanoate/water/heptane[13] and decylamine-undecenoic acid/water/decane.[14] For none of these systems, the microstructure of the reverse

* To whom correspondence should be addressed. E-mail: benjamin.abecassis@cea.fr (B.A.); fabienne.testard@cea.fr (F.T.).
† LIONS.
‡ The Royal Veterinary and Agricultural University.
§ Institut Laue-Langevin.

(1) Jokela, P.; Jonsson, B.; Khan, A. *J. Phys. Chem.* **1987**, *91*, 3291−3298.
(2) Kaler, E.; Murthy, A.; Rodriguez, B.; Zasadzinski, J. *Science* **1989**, *245*, 1371.
(3) Schubert, B. A.; Kaler, E. W.; Wagner, N. J. *Langmuir* **2003**, *19*, 4079−4089.
(4) Zemb, T.; Dubois, M.; Deme, B.; Gulik-Krzywicki, T. *Science* **1999**, *283*, 816−819.
(5) Dubois, M.; Deme, B.; Gulik-Krzywicki, T.; Dedieu, J. C.; Vautrin, C.; Desert, S.; Perez, E.; Zemb, T. *Nature (London)* **2001**, *411*, 672−675.
(6) Dubois, M.; Lizunov, V.; Meister, A.; Gulik-Krzywicki, T.; Verbavatz, J. M.; Perez, E.; Zimmerberg, J.; Zemb, T. *Proc. Natl. Acad. Sci. U.S.A.* **2004**, *101*, 15082−15087.
(7) Dubois, M.; Gulik-Krzywicki, T.; Deme, B.; Zemb, T. *C. R. Acad. Sci.* **1998**, *9*, 567−575.
(8) Zemb, T.; Dubois, M. *Aust. J. Chem.* **2003**, *56*, 971−979.
(9) Kaler, E.; Herrington,; Murthy, A.; Zasadzinski, J. *J. Phys. Chem.* **1992**, *96* (16), 6698−6707.
(10) Marques, E.; Regev, O.; Khan, A.; Lindman, B. *Avd. Colloid Interface Sci.* **2003**, *100−102*, 83−104.
(11) Khan, A.; Marques, E. F. *Curr. Opin. Colloid Interface Sci.* **1999**, *4*, 402−410.
(12) Jonsson, B.; Jokela, P.; Lindman, B.; Sadaghiani, A. *Langmuir* **1991**, *7*, 889−895.
(13) Friman, R.; Backlund, S.; Hognesen, E.; Austad, T. *Tenside Surf. Det.* **2004**, *41*, 190−194.
(14) Zhu, B.; Shi, H.; Huang, J.; He, X. *Acta Chimi. Sin.* **2001**, *59*, 913−917.

10.1021/la061465r CCC: $33.50
Published on Web 08/16/2006

microemulsion phase was determined precisely. Khan et al.[15] showed that w/o microemulsions are absent for a catanionic surfactant with a large polar headgroup and present for a catanionic surfactant with small headgroup depending on the temperature. Li and Kunieda[16] reviewed the solubilization and microemulsion formation for systems containing catanionic surfactants and alcohols. They discuss the three-phase behavior of these microemulsions and link the solubilization capacity to the distribution of the mixed surfactant at the interface.

In the present project, we focus on the water poor region of the phase diagram. This is the domain of a special type of microemulsions called reverse micelles.[17] Microemulsions are isotropic, clear, and thermodynamically stable fluids consisting of a mixture of oil, water, and surfactant. Depending on composition (concentration in surfactant, water-to-surfactant ratio, and ionic strength of the water phase) or thermodynamics (temperature), different microstructures and topologies can be observed. These belong to four classes which can be identified by combined conductivity and scattering studies made along dilution lines: isolated droplets (either spherical or rodlike), random bicontinuous, connected cylinders, and connected bilayers.

The microstructure and phase behavior of the microemulsion also depend on the properties of the surfactant film through the values of the spontaneous curvature, the bending modulus κ, and the saddle splay modulus $\bar{\kappa}$. Nonionic surfactants (such as C_iE_j from the *n*-alkyl polyglycol ether) are known to have spontaneous curvature which strongly depends on the temperature[18] and a curvature energy close to *kT*. The surfactant film is flexible and can easily depart from the spontaneous curvature. For rigid systems, the energy cost due to curvature change is too high, and the effect of temperature is much less pronounced. This is the case of DDAB or AOT. Lecithin is a particular and interesting case as it has been shown[19−22] that, in alkanes, this zwitterionic phospholipid self-assembles into long wormlike chains in the presence of small amounts of water. This kind of giant micelle is often observed in a direct system, but reports showing the presence of reverse wormlike micelles in oil are fewer.[23] Their structure resembles that of a linear polymer as the surfactant self-assembles into long (eventually entangled) semi-flexible chains. The main difference is that the different "monomers" are linked together by weak forces which are of the order of magnitude of *kT* instead of strong covalent bonds. Their dynamic behavior should also differ as the polymeric chains are continuously forming and breaking. The increase of the micellar length in these living polymers is often triggered by a suitable control parameter such as temperature,[24] ionic strength,[25] or addition of a cosurfactant.[26]

In the present paper, we present a systematic study to determine the shape and topology of the reverse microemulsion in the octylammoniumoctanoate (C8N8)/water/octane system. With small angle-neutron scattering, dynamic light scattering, and conductivity experiments, the effect of concentration and water-to-surfactant ratio are investigated. We concentrate on the case of equimolarity of the cationic and anionic surfactants such that no structural charges are present in the system. The questions adressed in this paper are the following: First, at equimolarity, are w/o microemulsions made with relatively short chains closer to stiff or rigid microemulsions? Second, is there a local microstructure in one of the canonic forms such as micelles, random bicontinuous dispersions, connected cylinders, or connected bilayers? Third, is the spontaneous curvature of a neutral catanionic surfactant film varying with temperature, as with other nonionic surfactants?

2. Experimental Section

2.1. Chemicals. Octanoic acid (99.5%), octylamine (99%), and octane (99%) were purchased from Sigma-Aldrich. Deuterated octane (98%) was purchased from Eurisotop (France). Deionized water from a Milli-Q purification system (Millipore, USA) of resistivity 18.2 MΩ.cm was used in preparing samples.

2.2. Sample Preparation. The catanionic surfactant is obtained by mixing equal quantities of octanoic acid and octylamine in diethyl ether followed by evaporation of the solvent under vacuum. A white powder is obrained.[12] To prepare a microemulsion, a given quantity of (deuterated) alkane, water, and catanionic surfactant are weighted in a Teflon screw cap vial and vortex mixed. A clear, low viscosity solution is obtained. For the conductivity and dynamic light scattering experiment, hydrogenated octane is used. For the SANS experiments, deuterated octane is used while keeping the catanionic surfactant and the water hydrogenated. A microemulsion can be completely defined by two parameters: the overall surfactant concentration and the water to surfactant molar ratio (denoted respectively as *c* and R_w). Unless otherwise stated, octane is used as the alkane. The volume fraction are comprised between 0.8% for the 0.05 M samples to 15% for the 0.8 M sample

2.3. Phase Behavior Determination. The maximal amount of water which can be incorporated by a given microemulsion is found by mixing a solution of catanionic surfactant in octane at a given concentration with a pure phase of water. The biphasic sample is then vortex mixed and set to rest at the given temperature overnight. The amount of water in the microemulsion phase is then determined by Karl Fischer titration.

2.4. Conductivity Measurements. Conductivity measurements are performed using a METTLER DL77 titrator coupled to a TACUSSEL CD810 conductimeter. Small amounts of water or octane are automatically added to a given microemulsion under magnetic agitation. The time between the addition of water and the measurement is 1 min. To check that no kinetic artifacts perturb the measurement, several microemulsions of different water-to-surfactant ratios, R_w, are prepared and equilibrated for 1 day before the conductivity measurement was performed. The difference of conductivity between the two methods are within the precision of the conductimeter.

2.5. Molecular Volume Determination. The density of different surfactant solutions with different mass fractions *x*, are measured with an Anton Paar DMA 5000 density meter. The slope of the curve $1/\rho$ versus *x*, gives the partial specific molecular volume of the solute as

$$\frac{1}{\rho} = \frac{1}{\rho_0} + x\left(\frac{V_2}{M_2} - \frac{1}{\rho_0}\right) \quad (1)$$

where ρ_0 is the solvent density, ρ is the solution density, V_2 is the molar volume of the solute, and M_2 is the molar weight of the solute. The molecular volume was found to be 520 Å^3 for the catanionic mixture meaning a 260 Å^3 per surfactant molecule. The molecular volume of water is 30 Å^3.

2.6. Small Angle Neutron Scattering. For the small angle scattering measurements, the microemulsions are transferred to

(15) Khan, A.; Marques, E. In *Specialist Surfactant*; Robb, I., Ed.; Blackie Academic and Professional: London, 1997; Chapter 3.
(16) Li, X.; Kunieda, H. *Curr. Opin. Colloid Interface Sci.* **2003**, *8*, 327−336.
(17) Zulauf, M.; Eicke, H. *J. Phys. Chem.* **1979**, *83*, 480−486.
(18) Strey, R. *Ber. Bunsen-Ges. Phys. Chem.* **1996**, *100*, 182.
(19) Schurtenberger, P.; Jerke, G.; Cavaco, C. *Langmuir* **1996**, *12*, 2433−2440.
(20) Jerke, G.; Pedersen, J. S.; Egelhaaf, S. U.; Schurtenberger, P. *Phys. Rev. E* **1997**, *56*, 5772-.
(21) Angelico, R.; Olsson, U.; Palazzo, G.; Ceglie, A. *Phys. Rev. Lett.* **1998**, *81*, 2823−2826.
(22) Angelico, R.; Ceglie, A.; Olsson, U.; Palazzo, G. *Langmuir* **2000**, *16*, 2124−2132.
(23) Yu, Z.-J.; Neuman, R. D. *Langmuir* **1994**, *10*, 2553−2558.
(24) Duval, M.; Waton, G.; Schosseler, F. *Langmuir* **2005**, *21*, 4904−4911.
(25) Khatory, A.; Kern, F.; Lequeux, F.; Appell, J.; Porte, G.; Morie, N.; Ott, A.; Urbach, W. *Langmuir* **1993**, 933−939.
(26) Stradner, A.; Glatter, O.; Schurtenberger, P. *Langmuir* **2000**, *16*, 5354−5364.

Hellma quartz cells (1 or 2 mm thick) and placed in a thermostated sample holder. The measurements are performed on the D22 and D11 instruments at the ILL (Institut Laue Langevin, Grenoble, France). Three (D22) or four (D11) different combinations of collimation lengths and sample-to-detector distances were used in order to cover wide range of scattering vectors and to get a sufficiently good overlapping between the data set from the different configurations. The resolution effects are relatively small on this instrument but are nevertheless taken into account in the data analysis using the approach described in ref 27. The scattering spectra were azimuthally averaged, background subtracted and converted to an absolute scale using the standard procedures of the respective instruments.

2.7. Dynamic Light Scattering. Dynamic light scattering measurements are made on an instrument from Brookhaven Instruments using the BI9000AT digital correlator and a 514.5 nm Argon ion laser. The glass vial containing the microemulsion is placed in a thermostated sample holder filled with the refractive index matching liquid Decalin. The sample is kept at 298 K 15 min prior to measurements. The autocorelation function is measured during 30 s and fitted by a biexponential function. Each measurement is repeated 5 times and the reported values are the averaged hydrodynamic radii.

3. Theory and Methods of SANS Data Analysis

3.1. Indirect Fourier Transform. In small-angle scattering the intensity I is measured as a function of the length of the scattering vector $q = 4\pi \sin(\theta)/\lambda$, where λ is the wavelength of the radiation and θ is half the scattering angle. For scattering from a dilute solution of particles of maximum dimension d, the intensity can be written in terms of the pair distance distribution function (PDDF) $p(r)$[28]

$$I(q) = 4\pi \int_0^{D_{\max}} p(r) \frac{\sin(qr)}{qr} \, dr \qquad (2)$$

For particles of uniform scattering length density, the distance distribution function $p(r)$ is proportional to the probability distribution for the distance between two arbitrary scattering points within the particle.

The aim of the indirect Fourier transformation (IFT) is to restore $p(r)$, which by virtue of the Fourier transformation contains the full information present in the scattering profile.

Many methods for estimation of the distance distribution function have been suggested,[29−31] but the most frequently used method is that of Glatter.[29] Using this method, the scattering profile is fitted to some sensible level while simultaneously the curvature of the estimated distance distribution is kept as low as possible. This is intended to give the PDDF of the lowest informational content (featureless appearance) that fits the data adequately.

In the present paper, the method as initially proposed by Glatter has been used. Applying the rules of probablity theory to the method of Glatter results in some minor modifications which have also been implemented in the analysis.[32]

3.2. Detailed Micelle Structures as Determined by Modelfits of the SANS Data. Based on the results of the indirect Fourier transform analysis (see more details later), we conclude that, depending on surfactant concentration and R_w, the shapes of the micelles are either spherical, ellipsoidal/short cylindrical, or long and wormlike. We have used this information to develop geometrical models for the micelles that have been fitted to the SANS data. The models include the relevant molecular constraints and mass conservation constraints.

We have assumed that the spherical micelles are polydisperse and that their size distribution can be described by a Gaussian. The data from the elongated micelles have been fitted with models for, respectively, short rigid cylinders and long semiflexible cylinders. We find the best fits to the scattering data from these elongated micelles when we use an elliptical cross-section of the cylinders. This is consistent with previous findings.[33−35]

A polydispersity of the length of the cylindrical micelles was not included in the present analysis. Multiple chemical equilibrium theory for cylindrical micelles predicts a significant polydispersity of the length of the micelles. However, previous studies of dense solutions of wormlike micelles conclude that, in the small-angle scattering data, the effect of the length-distribution of the micelles is small as compared to the effects of intermicellar interactions.[34,36] Since these two effects are present in the same q range, we are unable to extract information about the length-distribution of the micelles from the scattering data.

The small-angle scattering, $I(q)$, from a suspension of micelles may generally be expressed as[37,38]

$$I(q) = \phi \, V \, \Delta\rho^2 P(q) \, S(q) \qquad (3)$$

ϕ is the volume fraction of the micelles and is, for our system, straightforward to calculate from the concentrations of surfactant and water and their partial specific molecular molecular volumes. V is the volume of a single micelle. For the spherical micelles, $V = 4/3\pi R^3$, where R is the micelle radius. For the short rigid and the long semiflexible cylindrical micelles, $V = \pi\epsilon R^2 L$, where R is the minor axis of the elliptical cross-section, ϵ is the axis ratio and L is the contour length of the cylinders. For the modeling of the micelles, we assumed that the scattering length density of the micelles is homogeneous and equal to the average scattering length density of the catanionic surfactant, that is $\rho = -0.068 \times 10^{10}$ cm^{-2}. The micelles are seen on a background of deuterated octane having a scattering length density of $\rho = 6.37 \times 10^{10}$ cm^{-2}. Thus, the excess scattering length density, $\Delta\rho$, of the micelles equals 6.44×10^{10} cm^{-2}. $P(q)$, the scattering form factor, describes the q dependence of the scattering from the single micelles. $P(q)$ is normalized such that $P(q) = 1$ for $q = 0$. $S(q)$, the structure factor, describes the effects of the micelle−micelle interactions (e.g., excluded volume effects) on the scattering pattern. These are described in more detail in the following.

Scattering Form Factors. The scattering form factor for the spherical micelles is given by[37]

$$P(q) = \left(\frac{3[\sin(qR) - qR\cos(qR)]}{(qR)^3} \right)^2 \qquad (4)$$

where R is the radius of the micelles. In the model fits, a polydispersity of the spherical micelles is taken into account by

(27) Pedersen, J. S.; Posselt, D.; Mortensen, K. *J. Appl. Crystallogr.* **1990**, *23*, 321−333.
(28) Glatter, O. In *Small-Angle X-ray Scattering*; Glatter, O., Kratky, O., Eds.; Academic Press: London, 1982.
(29) Glatter, O. *J. Appl. Crystallogr.* **1977**, *10*, 415−421.
(30) Svergun, D. I.; Semenyuk, A. V.; Feigin, L. A. *Acta Crystallogr.* **1988**, *A44*, 244−250.
(31) Hansen, S.; Pedersen, J. *J. Appl. Crystallogr.* **1991**, *24*, 541−548.
(32) Hansen, S. *J. Appl. Crystallogr.* **2000**, *33*, 1415−1421.
(33) Bergström, M.; Pedersen, J. S. *Phys. Chem. Chem. Phys.* **1999**, *1*, 4437−4446.
(34) Arleth, L.; Bergstrom, M.; Pedersen, J. S. *Langmuir* **2002**, *18*, 5343−5353.
(35) Arleth, L.; Bauer, R.; Ogendal, L. H.; Egelhaaf, S. U.; Schurtenberger, P.; Pedersen, J. S. *Langmuir* **2003**, *19*, 4096−4104.
(36) Garamus, V. M.; Pedersen, J. S.; Kawasaki, H.; Maeda, H. *Langmuir* **2000**, *16*, 6431−6437.
(37) Lindner, P., Zemb, T., Eds.; *Neutrons, X.-Rays and Light: Scattering Methods Applied to Soft Condensed Matter*; North-Holland: Amsterdam, 2002.
(38) Hayter, J. B.; Penfold, J. *J. Chem. Soc., Faraday Trans. 1* **1981**, *77*, 1851−63.

averaging eq 3 over a Gauss distribution so that the fitted expression for the spherical micelles becomes

$$I(q) = \phi\, \Delta\rho^2 \int_{R_{min}}^{R_{max}} N(R)\, V(R)\, P(q, R)\, S(q)\, \mathrm{d}R \qquad (5)$$

where $V(R)$ is the volume of a sphere with radius R and where $N(R)$ denotes the Gauss distribution

$$N(R) = \frac{1}{\sqrt{2\pi}\,\sigma\bar{R}} \exp\left[-\frac{(R-\bar{R})^2}{2(\sigma\bar{R})^2}\right] \qquad (6)$$

where $\bar{R}$ is the average radius of the micelles, $\sigma\bar{R}$, is the standard deviation so that σ becomes the relative standard deviation which we will also refer to as the polydispersity.

The scattering form factor for the short rigid cylindrical micelles with elliptical cross-section is given by[37]

$$P(q) = \frac{2}{\pi}\int_0^{\pi/2}\int_0^{\pi/2}\left[\frac{2J_1(qR(\epsilon,\phi,\alpha))}{qR(\epsilon,\phi,\alpha)} \times \frac{\sin(qL\cos\alpha/2)}{qL\cos\alpha/2}\right]\mathrm{d}\phi\,\sin\alpha\,\mathrm{d}\alpha \qquad (7)$$

where R is the minor axis and ϵR is the major axis of the elliptical cross-section and $R(\epsilon,\phi,\alpha) = [(\epsilon R)^2 \sin^2\phi + R^2\cos^2\phi]^{1/2}\sin\alpha$. $J_1(x)$ is the first-order Bessel function of the first kind. The integrations over ϕ and α have to be carried out numerically.

When the micelles are sufficiently long, $L > 10R$, the micelles may be described by an expression which separates $P(q)$ into a cross-sectional contribution, $P_{CS}(q)$, and a longitudinal contribution. For semiflexible "wormlike" micelles, the longitudinal contribution is denoted $P_{WC}(q)$

$$P(q) = P_{CS}(q)P_{WC}(q) \qquad (8)$$

$P_{CS}(q)$ is for micelles with an elliptical cross-section given by[37]

$$P_{CS}(q) = \frac{2}{\pi}\int_0^{\pi/2}\left[\frac{2J_1(qR(\epsilon,\theta))}{qR(\epsilon,\theta)}\right]^2 \mathrm{d}\theta \qquad (9)$$

The integration over θ has to be carried out numerically.

A numerical expression for the longitudinal contribution from wormlike micelles was developed by Pedersen and Schurtenberger.[39] The expression is based on a series of Monte Carlo simulations of semiflexible polymers and wormlike micelles with excluded volume effects. The polymer configurations have been sampled and the scattering functions calculated.[39,40] Furthermore, the scattering functions have been parametrized numerically using the procedure by Yoshizaki and Yamakawa.[41] This leads to expressions for the scattering functions which can be used in the analysis of small-angle scattering data from semi-flexible polymers or wormlike micelles[39]

$$F_{WC}(q, L, b) = [(1 - \chi(q, L, b))F_{chain}(q, L, b) + \chi(q, L, b)F_{rod}(q, L)]\Gamma(q, L, b) \qquad (10)$$

where L is the contour length of the micelles and b is the Kuhn length. $F_{chain}(q, L, b)$ denotes the scattering function for a flexible chain with excluded volume effects which is given by an empirical expression (eq 13 in ref 39). $F_{rod}(q, L)$ denotes the scattering function of an infinitely thin rod (eq 6 and 7 in ref 39). The mathematical expression for $F_{rod}(q, L)$ was originally derived by Neugebauer.[42] At low angles, $F_{chain}(q, L, b)$ dominates the scattering pattern, and at higher angles, $F_{rod}(q, L)$ dominates. In the crossover region, the scattering is given by a combination of $F_{chain}(q, L, b)$ and $F_{rod}(q, L, b)$. In the expression $\chi(q, L, b)$ is a crossover function, and $\Gamma(q, L, b)$ is a function which corrects the crossover region.[39,41]

Rounded end caps could be included in the model and might provide a more physical description. However, we have found that the effect of sharply cut off cylinder ends instead of rounded ends is not significant in the overall scattering pattern, and instead, we use the more simple model of (flexible) cylinders with sharply cut off ends. Similar model fitting procedures have previously been used on other systems. See for example refs 20, 33−36, 43, and 44.

Structure Factors. Our IFT analysis indicated that effects of particle−particle interactions are only of minor importance for the spherical and short cylindrical micelles at the relevant concentrations. Therefore, we decided to omit the $S(q)$ in the analysis of the spherical micelles and short cylindrical micelles by simply setting $S(q) = 1$. However, for the long semiflexible micelles formed at high concentrations and high R_w, the particle−particle interactions become important. We have modeled the structure factor $S(q)$ using the approach based on the polymer reference interaction site model (PRISM) that we have also used in previous work.[34,35] The PRISM expression calculated in the equivalent site approximation for thin chains[45] leads to the following expression for the structure factor of the wormlike micelles

$$S(q) = \frac{1}{1 + \nu(X)c(q)P_{WC}(q)}$$

where $\nu(X)$ is related to the concentration of the micelles, X refers to the reduced concentration, and $c(q)$ is the normalized Fourier transform of the direct correlation function corresponding to the correlation hole arising along the chain if the chain has a finite radius (see further details in refs 34, 35, and 45). Unfortunately, the information about the length of the micelles and the structure factor parameters are present in the same low-q region of the experimental scattering function. This implies that the structure factor parameters, the contour length, and in some cases also the Kuhn length are coupled when the PRISM model for the semiflexible wormlike micelles is fitted to the scattering data. In refs 34 and 35, we solved this problem by first determining the Kuhn length and a growth-law for the micelles from the low concentration data (where $S(q)$ could be ignored). Second, we apply the obtained Kuhn length and growth law in order to determine the $S(q)$ parameters from the high concentration data. A similar approach might be applied for the reverse wormlike micelles formed in the octylammonium-octanoate/octane water system. However, even though our light scattering data give us some indication of the growth law of the reverse micelles, we do not yet have sufficiently detailed data to use the approach we used in refs 34 and 35. On the other hand, reliable fits to our SANS data, including the high-q part of the data, can also not be fitted without including a model for the structure factor. As a compromise, we have used the PRISM approach 3.2 to take into account the structure factor effects at low-q in the scattering data. This way we can conclude whether the SANS data are

(39) Pedersen, J.; Schurtenberger, P. *Phys. Rev. E* **1996**, *54*, R5917−R5920.
(40) Pedersen, J. S.; Schurtenberger, P. *J. Appl. Crystallogr.* **1996**, *29*, 646−661.
(41) Yoshizaki, T.; Yamakawa, H. *Macromolecules* **1980**, 1518−1525.
(42) Neugebauer, T. *Ann. Phys. (Leipzig)* **1943**, *42*, 509−533.
(43) Pedersen, J. S.; Egelhaaf, S. U.; Schurtenberger, P. *J. Phys. Chem.* **1995**, *99*, 1299−1305.
(44) Magid, L. J.; Li, Z.; Butler, P. D. *Langmuir* **2000**, *16*, 10028−10036.
(45) Pedersen, J.; Schurtenberger, P. *Europhys. Lett.* **1999**, *45*, 666−672.

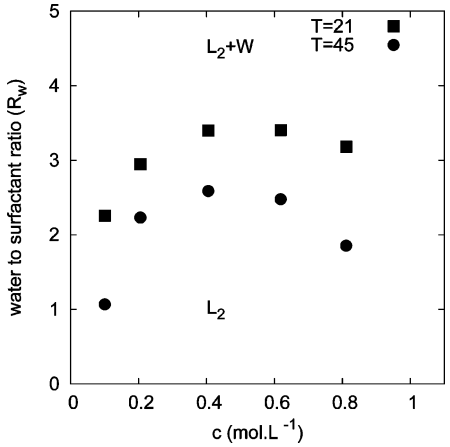

Figure 1. Maximum water solubilization (emulsification failure) R_w in the L_2 phase for two different temperatures.

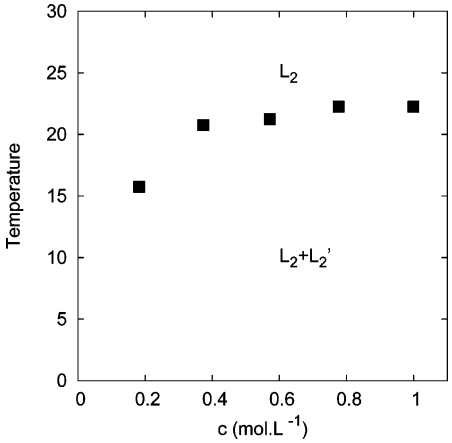

Figure 2. Phase diagram indicating the $L_2 + L_2'$ phase separation temperature for $R_w = 2$ at various concentrations c.

well-described by our wormlike micelle model. Unfortunately, the coupling between the fit-parameters determined from the low-q data implies that we can only determine a minimal value of the contour length of the wormlike micelles. It should also be stressed that a possible effect of a branching or junctions points of the wormlike micelles is not taken into account in the present model. To our knowledge, there are no analytical models that accounts for the effect. However, a branching of the cylindrical micelles will correspond to an increase of the fractal dimension, f of the micellar structures, which again will be reflected in the small-angle scatttering pattern as a q^{-f} power-law behavior at the length scale of the branching (Zemb in ref 37). The low-q scattering from un-branched wormlike micelles with excluded volume effects decreases as $q^{-5/3}$. Therefore, a power-law behavior with an exponent higher than the 5/3 should be obtained from branched wormlike chains such as it is the case for star polymers (ref 46 and Pedersen in ref 37). Actually, a form factor with a q^{-2} power-law behavior[47] has been predicted for the branched structure of Tlusty et al.[48]

4. Results

4.1. Phase Behavior. Two different phase instabilities are observed in the reverse micellar domain of this system. The first one is the classical emulsification failure. When small amounts of water are added to the neat surfactant−oil mixture, a microemulsion forms. However, as more and more water is added, at some point, the system phase separates into a water-saturatated microemulsion and an excess water phase. This value is reported as a function of concentration, c, and for two different temperatures in the phase diagram in Figure 1. An obvious feature of this system is that it only solubilizes a low amount of water as compared to some specially developed "balanced" surfactants such as the anionic AOT or DDAB. At low temperature, the amount of water which can be incorporated is larger than at high temperature, but the trend in the variation with the concentration is the same at the two studied temperatures.

The other observed phase separation appears only at certain surfactant concentrations ($C = 0.2-0.8$ M), for low water-to-surfactant ratios and with decreasing temperature. In this case, the fluid separates into two distinct microemulsions in equilibrium. The temperature at which this phase transition occurs is indicated in Figure 2 as function of the concentration. A dense lower phase containing most of the water (as controlled by Karl Fischer titration) and an upper phase which is almost exempt of water. We must stress that this phase instability is different from the emulsification failure where a pure phase of the "inner" content is rejected and stays in equilibrium with a saturated microemulsion. As just noted, the second type of phase separation occurs when the temperature is decreased. For example, a sample of composition 0.8 M and $R_w = 2$ (in octane) phase separates when the temperature is decreased below 22 °C. The volume of the lower dense increases when the water-to-surfactant ratio is increased. The lower dense phase is of high viscosity as compared to the single phase microemulsion but no birefringence is observed.

Table 1. Temperature at Which the $L_2 + L_2'$ Phase Separation Occurs Depending on the Nature of the Oil for a Concentration in Surfactant of 0.4 M and $R_w = 2$

solvent	phase separation temperature
hexane	6
isooctane	21
octane	23
decane	41

Increasing the ionic strength of the "water" inner phase has the same effect on the phase behavior as a decrease in temperature. For example, when a 0.5 M aqueous solution of $BaCl_2$ is used, a phase separation is observed at 25 ° C for $c = 0.4$ M and $R_w = 2$, whereas the same sample with pure water is monophasic.

The temperature at which the second type of phase separation occurs depends strongly on the nature of the oil which is used as a solvent. The phase separation temperatures are reported in Table 1 for hexane, isooctane, octane, and decane. All measurements were made with a concentration of surfactant of 0.4 M and a water-to-surfactant ratio of 2. As may be seen from the table, the phase separation temperature strongly increases as the length of the alkane chain is increased. The explanation of this systematic trend is that the phase separation temperature depends on the ability of the oil to penetrate the surfactant palisade. The more penetrating the oil, the lower the transition temperature.

4.2. Conductivity Measurements. Figure 3 shows conductivity measured along the water dilution line for three different surfactant concentrations. The reduced conductivity, κ/c, where κ is the conductivity and c is the surfactant concentration is plotted as a function of the water-to-surfactant ratio R_w. Addition of water is stopped at the emulsification failure, i.e., when excess water in equilibrium with the microemulsion started to be present. The data show that the conductivity increases steeply as R_w is increased up to $R_w \sim 2$. For $R_w > 2$, the conductivity reaches a plateau before the phase separation takes place.

(46) Benoit, H.; Doty, P. J. *J. Phys. Chem.* **1953**, *57*, 958.
(47) Zilman, A.; Safran, S. *Phys. Rev. E* **2002**, *66*, 51107−51134.
(48) Tlusty, T.; Safran, S.; Strey, R. *Phys. Rev. Lett.* **2000**, *84*, 1244−1247.

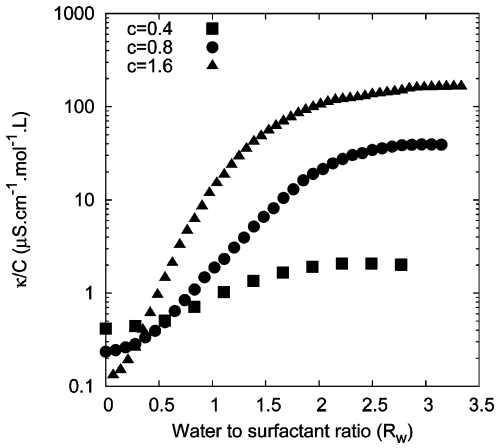

Figure 3. Normalized conductivity along water dilution line for different surfactant-to-oil ratio in C8N8/water/octane L_2 phase. Measurements are obtained at 25 °C. The concentrations are in mole per liter.

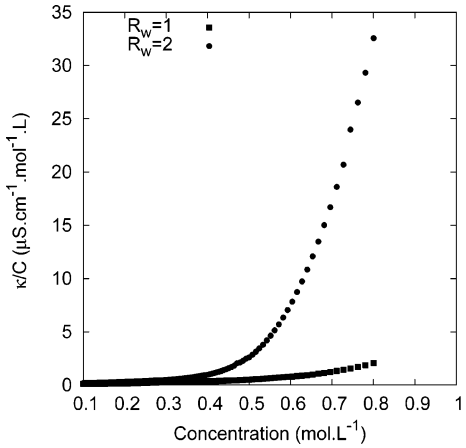

Figure 4. Normalized conductivity measured along the oil dilution line in the L_2 phase for $R_w = 1$ and 2 at 25 °.

Figure 4 shows conductivity measured along the oil dilution line within the L_2 phase. The data show that the way the conductivity is varying with dilution also depends strongly on the water-to-surfactant ratio. For $R_w = 1$, the normalized conductivity is almost constant for concentrations ranging from 0.1 to 0.6 M and increases only slightly from 0.6 to 0.8 M, whereas for $R_w = 2$, a strong increase in conductivity is observed already at $c = 0.3$ M. This indicates that the degree of connectivity of the micelles may increase in this part of the concentration range.

The temperature dependence of the conductivity is also measured. Figure 5 shows the result obtained for the $c = 0.8$ M and $R_w = 2$ sample in octane. A strong decrease of the conductivity is observed as the temperature increases. This indicates that the micelles become less connected with increasing temperature.

4.3. Small-Angle Neutron Scattering. *Visual Inspection of Scattering Data and Pair-Distance Distribution Functions.* Examples of small angle neutron scattering data, $I(q)$ and the corresponding $p(r)$'s for two different surfactant concentrations and with varying R_w are presented in Figures 6 ($c = 0.2$ M) and 7 ($c = 0.8$ M). The data clearly show that heterogeneities in the scattering length densities are present in our system; hence, we conclude that self-assembly occurs and the scattering signal is produced by the contrast between the protonated reverse micelles and the deuterated solvent oil. For all concentrations, addition of water induces a growth of the scattering intensity at low q. As this growth is much too large to be explained by the small

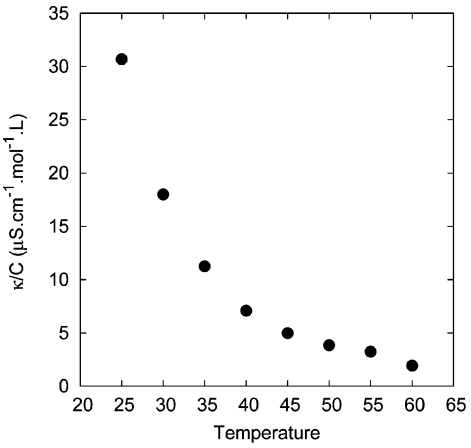

Figure 5. Normalized conductivity as a function of temperature for a sample of composition $c = 0.8$ M and $R_w = 2$

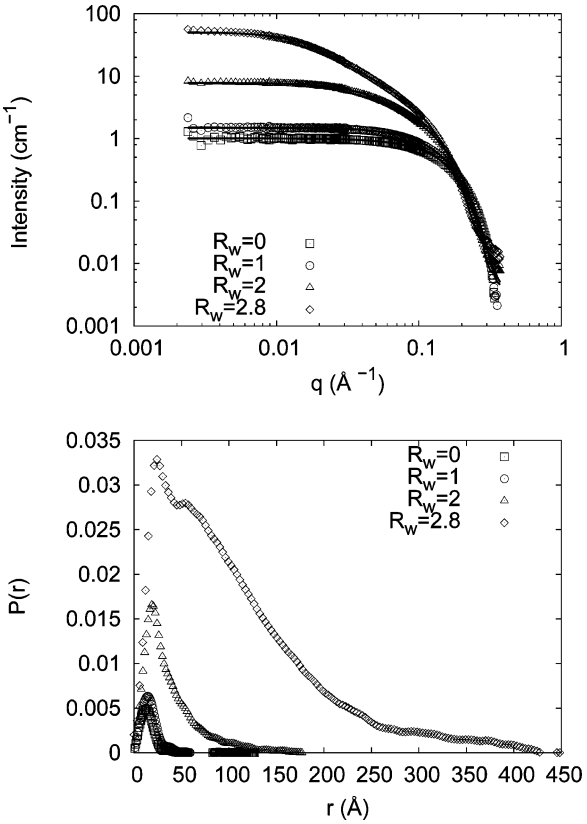

Figure 6. SANS diagram and $p(r)$ obtained along a water dilution line in a C8N8/water/octane L_2 phase at $c = 0.2$ M.

increase of the volumes of the scattering micelles, we conclude that either the size of the single micelles or the attraction between them increases (or a combination of the two).

The scattering data measured at low values of R_w (see e.g. $R_w = 0$ and 0.9 for the 0.2 M sample, Figure 6) are characteristic of rather small spherical micelles (see e.g. Chapter 4 of ref 37). This interpretation is supported by the corresponding pair-distance distribution functions which have a nearly perfect bell-shape as expected for spherical particles (ibid). A closer examination of these $p(r)$ functions gives a D_{max} of ~30 Å for practically all of the scattering data that indicates spherical micelles. The D_{max} is the maximal distance measured within the scattering particles; thus, for the spherical micelles, a D_{max} of 30 Å corresponds to a maximal diameter of 30 Å or a radius of 15 Å.

At slightly higher values of R_w (see e.g. $R_w = 2$ for the $c = 0.2$ M sample, Figure 6), a q^{-1} slope is visible at intermediate

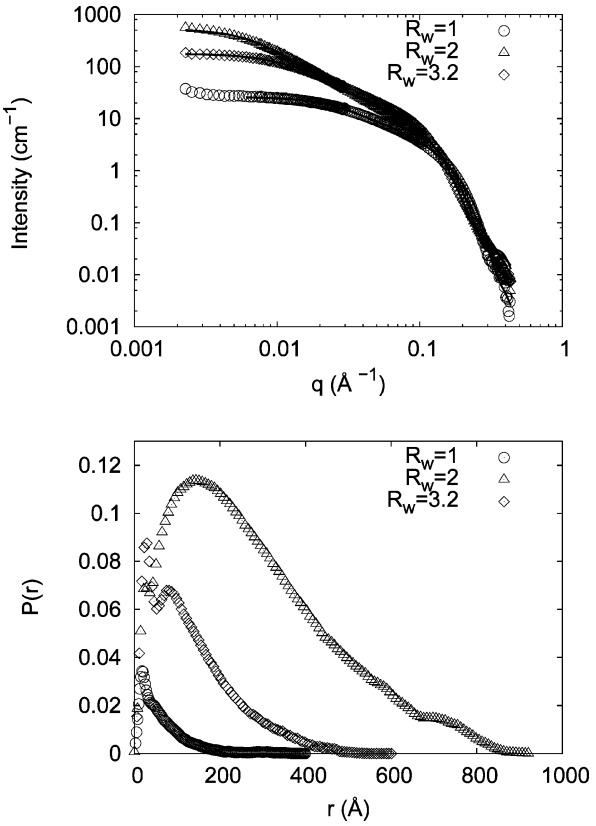

Figure 7. SANS diagram and $p(r)$ obtained along a water dilution line in a C8N8/water/octane L_2 phase at $c = 0.8$ M

q values ($q \approx 0.03-0.1$ Å^{-1}). This scattering behavior is an indication that rigid cylindrical micelles are formed (ibid). This interpretation is again supported by the corresponding pair distance distribution functions. These keep the bell-shaped peak at low r values, but exhibit a slow decrease, also referred to as a tail, at higher r values. This $p(r)$ shape is typical for cylindrical/rodlike particles. The bell-shaped part of the $p(r)$ observed at low r values may be attributed to pairs of scattering centers lying in the cross-section plane of the cylinders, whereas the tail may be attributed to pairs of scattering centers lying along the longitudinal axis of the cylinders. The D_{max} corresponds roughly to the length of the cylinders, whereas the position of the maximum of the $p(r)$ is related to the cross sectional diameter. For, example, the $p(r)$ of the $c = 0.2$ M and $R_w = 2$ sample show that these micelles are approximately 100 Å long and have a cross-sectional diameter of 30−35 Å. The sphere-to-rod transition of the micelles takes place at different water-to-surfactant ratios for the different overall surfactant concentrations. At low surfactant concentrations a relatively high R_w is required to induce the sphere-to-rod transition, while the higher the concentration, the less water is necessary to induce the transition.

At even higher values of R_w, the q^{-1} slope visible at intermediate q values ($q \approx 0.03-0.1$ Å^{-1}) bends over toward a $q^{-5/3}$ behavior at low q values ($q \approx 0.01-0.03$ Å^{-1}, see e.g. the $R_w = 2$ sample at $c = 0.8$ M). This is an indication that long semiflexible/wormlike micelles are formed.[43] The $p(r)$ functions support that large aggregates are formed. The $p(r)$ of the $R_w = 2$ sample at $c = 0.8$ M exhibits the remains of the rounded cylinder cross-section peak at low r values but otherwise exhibits a significant tail with a maximum/shoulder at ∼150 Å and a D_{max} of ∼800 Å. As it was observed for the relation between c, R_w, and the position of the sphere−rod transition, we observe that the higher the concentration, the less water is required to induce the formation of long semiflexible micelles. For concentrated samples (e.g. $c = 0.8$ M), a further increase of the water-to-surfactant ratio, which in this case reaches 3.2, leads to an apparent decrease in the length of the micelles as stated by a faster decrease of the pair distance distribution function. In this case, after an significant growth triggered by water addition, a further addition of water apparently induces the reverse effect. For lower concentrations, we do not observe this effect as the emulsification failure occurs before.

Results of Model Fits. To obtain more detailed and quantitative information about the micelles, the SANS data have been analyzed further with a model-fitting approach. The model for spherical micelles (see section 3.2) is fitted to the data corresponding to the low R_w values, the model for short rigid cylinders was fitted to the intermediate R_w data, and the model for the long semiflexible micelles is fitted to the high R_w data. For most of the data, however, at least two of the above-mentioned models are tested in order to determine what shape gave the best description of the actual micelles. The best model fits are plotted on top of the experimental data in Figures 6 ($c = 0.2$ M) and 7 ($c = 0.8$ M) and the results of the model fits are presented in Table 2.

It is seen from the plots that there is an excellent agreement between model fits and the experimental data in the entire q range. Thus, we conclude that the models give an adequate description of the micelles. When inspecting the results in Table 2, it is also obvious that the sphere-to-rod transition and the following increase of the length of the micelles are systematically promoted by both an increase of the total concentration of the micelles and an increase of the water-to-surfactant ratio, R_w.

For small R_w values and/or low c, we find that the model for polydisperse spherical micelles gives the best description of the data. The average radius of the spherical micelles remains nearly constant at 12−13 Å when either c or R_w increases (corresponding to moving from the upper left corner toward the lower right corner of Table 2); however, the polydispersity increases as the sphere-to-rod transition region is approached. It should be noted that the data from the spherical micelles could also be fitted with a model for prolate ellipsoidal micelles, and these fits suggested that the axis ratio of the micelles increased as the sphere-to-rod transition region is approached. The actual micelles are most likely both polydisperse and nonspherical and become more and more so as c or R_w increases. However, a separation of the polydispersity and the deviation from spherical cannot be made from our present data.

For intermediate values of R_w or c, we obtain the best fits with a model for short cylindrical micelles with an elliptical cross-section. As explained in section 3.2, the radius of the minor axis of the cross-section is R and the major axis is ϵR. The average cross-sectional radius we have reported in Table 2 is calculated from $R_{CS} = (\epsilon R^2)^{1/2}$. It is seen that the obtained R_{CS} of the short cylindrical micelles is comparable to the radius found for the spherical micelles. Furthermore, the obtained ellipticity of the cylinder cross-section is close to unity.

For large values of R_w or c, the model for long wormlike micelles with an elliptical cross-section is used to determine the detailed structure of the micelles. The intermediate to high-q part of the scattering data ($q > 0.1$ Å^{-1}) contains mostly information about the cross-sectional structure of the cylindrical micelles, that is the R_{CS} (defined in the same way as for the short cylinders) and the ellipticity of the cross-section, ϵ. These parameters are reported in Table 2. At low to intermediate q ($q < 0.1$ Å^{-1}), the information about the total length, L, of the micelles, their flexibility in terms of their Kuhn length, b, and the $S(q)$ are present. As mentioned previously, these may be coupled (see section 3.2 for further details). In the analysis of

Table 2. Fit Parameters as Determined from the Model Fits to the Scattering Data[a]

	0.05 M	0.1 M	0.2 M	0.4 M	0.6 M	0.8 M
$R_w = 0$		sphere $\bar{R} = 12.6$ Å $\sigma = 0.13$ $X_s = 1.0$	sphere $\bar{R} = 12.7$ Å $\sigma = 0.16$ $X_s = 0.82$	sphere $\bar{R} = 12.7$ Å $\sigma = 0.16$ $X_s = 0.97$		
$R_w = 1$		sphere $\bar{R} = 12.1$ Å $\sigma = 0.19$ $X_s = 0.73$	sphere $\bar{R} = 13.0$ Å $\sigma = 0.27$ $X_s = 0.81$	short cylinder $R_{CS} = 12.3$ Å $\epsilon = 1.30$ $L = 70$ Å $X_s = 0.83$	short cylinder $R_{CS} = 12.4$ Å $\epsilon = 1.21$ $L = 200$ Å $X_s = 0.78$	long wormlike $R_{CS} = 12.3$ Å $\epsilon = 1.50$ $L > 350$ Å $b = 120$ Å $X_s = 0.70$
$R_w = 2$	sphere $\bar{R} = 10.0$ Å $\sigma = 0.26$ $X_s = 0.73$	sphere $\bar{R} = 13.1$ Å $\sigma = 0.27$ $X_s = 0.82$	short cylinder $R_{CS} = 12.5$ Å $\epsilon = 1.29$ $L = 90$ Å $X_s = 1.12$	long wormlike $R_{CS} = 13.5$ Å $\epsilon = 1.48$ $L > 500$ Å $b = 100$ Å $X_s = 1.05$	long wormlike $R_{CS} = 15.0$ Å $\epsilon = 1.49$ $L > 1500$ Å $b = 103$ Å $X_s = 0.70$	long wormlike $R_{CS} = 14.1$ Å $\epsilon = 1.50$ $L > 2000$ Å $b = 93$ Å $X_s = 0.72$
$R_w = 3$	sphere $\bar{R} = 11.3$ Å $\sigma = 0.22$ $X_s = 0.72$	short cylinder $R_{CS} = 12.8$ Å $\epsilon = 1.0$ $L = 61$ Å $X_s = 1.0$	long wormlike $R_{CS} = 14.8$ Å $\epsilon = 1.56$ $L > 1000$ Å $b = 70$ Å $X_s = 1.27$		long wormlike $R_{CS} = 17.8$ Å $\epsilon = 1.67$ $L > 1200$ Å $b = 148$ Å $X_s = 0.82$	long wormlike $R_{cs} = 17.1$ Å $\epsilon = 1.70$ $L > 1200$ Å $b = 175$ Å $X_s = 0.73$

[a] Sphere: A model for polydisperse spherical micelles was fitted: $\bar{R}$ is the average radius, σ is the polydispersity, and X_s is the fitted scale factor. Short cylinder and long wormlike: The models for respectively, short cylindrical micelles and long wormlike micelles were fitted: R_{CS} is the average cross-sectional radius, ϵ is the axis ratio of the elliptical cross-section of micelles, and X_s is the fitted scale factor.

the present data, it turned out that the Kuhn length, b, of the semiflexible micelles was relatively short, separated out clearly in the scattering data, and gave rise to a $q^{-5/3}$ behavior extending out to relatively high q values. However, the contour length L and the $S(q)$ are generally coupled and from the present data and we can only report a lower limit for the length of the wormlike micelles in Table 2. Nevertheless, the analysis with the wormlike micelle model clearly confirms that the length of the micelles increases with both c and R_w. In the model fits, we generally found a Kuhn length of around 100 Å. However, our data for $R_w = 3$ and the $c = 0.6$ and 0.8 M indicate a slightly higher rigidity for these samples. The observation from the $p(r)$ functions of an apparent decrease of the micelle length at high concentrations and high R_w is confirmed by the model fits: We find a smaller minimum length in the $R_w = 3$ case than for $R_w = 2$ for the two highest concentrations studied. However, from the present data, we cannot conclude whether the effect is real or a result of increased intermicellar interactions for the longer micelles.

All of the data were fitted on an absolute scale; however, for all the fits, a scaling parameter, X_s, has to be multiplied to the theoretical model in order to obtain good fits. As may be seen from Table 2, X_s is relatively close to unity, but its magnitude varies slightly more from unity than what we can explain by the 10% uncertainty of the absolute scale calibration of the SANS data. The value of the X_s is to a very large extent determined by the model fit to the high-q region ($q > 0.06$ Å^{-1}). In the present case, the high-q scattering intensity is fully determined by the average radius of the micelles, the sample concentration, c, and the excess scattering length density, $\Delta\rho$. As we use a molecular constrained model, c and $\Delta\rho$ are fixed a priori. Thus, the only free parameter (except for X_s) is the average micelle radius, and as it turned out, it was necessary to fit X_s in order to obtain a sufficiently good fit at large q values. An explanation for the relatively low X_s values we find for most of the data may be that a small part of the surfactant resides in the solvent as an ion paired monomer. These molecules do not take part in the micelles and will not contribute to scattering. By assuming in the theoretical model that all the surfactant molecules are participating in the self-assembly, we thus overestimate the scattering intensity.

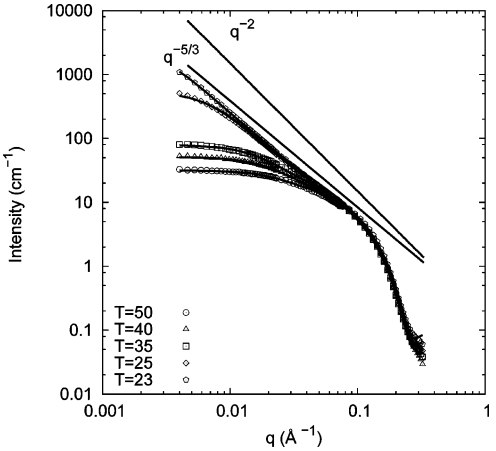

Figure 8. Scattering patterns of a L_2 phase of C8N8/water/octane system ($c = 0.8$M and $R_w = 2$) at various temperatures. Phase separation occurs at 23°.

Temperature Effects. To get further insight into the effect of temperature on this system, SANS data are measured at different temperatures for one of the samples ($c = 0.8$ M and $R_w = 2$). From the plot of the obtained data (see Figure 8), it is seen that the low-q scattering decreases significantly as temperature increases, whereas the scattering data at high-q remains unchanged. This strongly suggests that the length of the cylindrical micelles decreases as the temperature increases, whereas the cross-sectional radius of the micelles remains constant. This observation is confirmed by the model-fit analysis of the scattering data. The model for wormlike micelles was fitted to the scattering data and the results are summarized in Table 3. Our main observation is that the length of the micelles grow very fast as the temperature is decreased toward the phase separation temperature. The data from the temperature scan suggest that the cross-section radius and ellipticity of the micelles gets slightly

Table 3. Temperature Scan[a]

	R_{cs}, Å	e	L, Å	b, Å	X_s
$T = 23°C$	14.3	1.35	>4000	102	0.81
$T = 25°C$	14.6	1.43	>1500	113	0.71
$T = 35°C$	15.0	1.53	>500	150	0.76
$T = 40°C$	14.8	1.53	>300	250	0.75
$T = 50°C$	15.1	1.60	>200	250	0.86

[a] Fit parameters determined from the fits of the model for wormlike micelles to the scattering data from the $c = 0.8$ M, $R_w = 2.0$ sample measured at different temperatures.

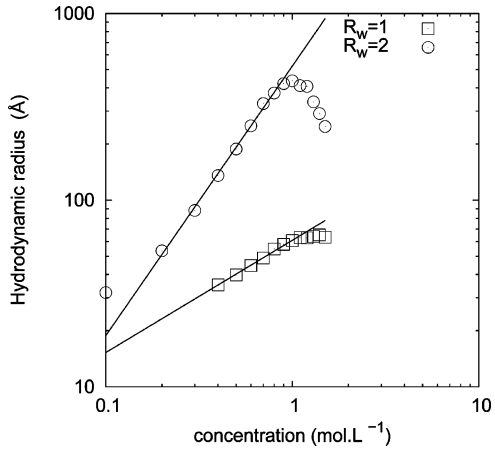

Figure 9. Hydrodynamic radius measured by dynamic light scattering for two R_w ratios along an oil dilution line in the L_2 phase.

smaller as temperature decreases and the micelles get longer. The data furthermore indicate that there is an inverse dependence between the Kuhn length of the micelles and their contour length. When the Kuhn length increases with increasing temperature, the micelles get shorter. A similar dependence between contour length and Kuhn length was observed in the study of the SDS wormlike micelles in ref 34. However, the dependence needs to be investigated in a dedicated study in order to be confirmed (or rejected).

When comparing Tables 2 and 3, it may be noted that the fit parameters for the $c = 0.8$ M, $R_w = 2$, $T = 25$ °C sample reported in the two tables are not exactly the same. The reported results are based on two different sample preparations, and the SANS data were measured at two different SANS instruments covering slightly different q ranges. However, comparing the data from these two different preparations and SANS measurements, it is seen that the reproducibility of our findings is very good.

4.4. Dynamic Light Scattering. To get more detailed insight into the growth behavior of the micelles, we measure their apparent hydrodynamic radius along an oil dilution line for two different water-to-surfactant ratios, $R_w = 1$ and 2. The data are reported in Figure 9.

For the $R_w = 1$ series in the studied concentration range, the SANS analysis shows that the micelles are spherical, short cylinders, or relatively short semiflexible micelles with a Kuhn length which is comparable to the contour length of the micelles. It is therefore fair to describe the micelles as rigid rods in which case $R_h \simeq R_g$, where R_h is the hydrodynamic radius and R_g, the radius of gyration, and[46]

$$R_g^2 = \frac{\bar{L}^2}{12} \tag{11}$$

where $\bar{L}$ is the average length of the rods. Thus $\bar{L} \propto R_h$ such that the $R_w = 1$ data suggest that the average length of the micelles grow proportionally to $c^{0.6}$. This is in good agreement with the mean field theory predictions[49]

$$\bar{L} \simeq c^{0.5}\exp(E/k_bT) \tag{12}$$

where E is the so-called scission energy of the chain (the energy required to create two chain ends). Scaling theory[49] predicts a slightly higher exponent (0.6) than a mean-field approach which is consistent with our experiment. The SANS analysis of the $R_w = 2$ series showed that the contour length quickly increases to values much larger than the Kuhn length. Thus, it is fair to describe the micelles as semiflexible or wormlike. For linear polymers in θ solvents, it has been found experimentally that $\sqrt{R_h} \propto M_w^{0.5}$, where the M_w is the molar mass of the polymers.[50] Thus, in the case of the linearly growing $R_w = 2$ micelles, we can assume that $\sqrt{R_h} \propto \bar{L}^{0.5}$ which, if combined with eq 12, would give a growth behavior comparable to $R_h \propto c^{0.25}$. We clearly observe a significantly larger growth exponent of 1.44 and conclude that the growth observed for the $R_w = 2$ micelles is much too fast to be explained by the mean field theory.[49]

5. Discussion

Two types of phase instabilities are observed in the system. The first one is the emulsification failure: it occurs when coexistence of a pure inner phase with the microemulsion is more stable than further increase of the inner phase content in a single phase microemulsion. A too large cost in bending energy for swelling of water droplets occurs when an excess of water is added to the binary surfactant/oil mixture. The second one is the liquid−gaslike phase transition: two microemulsions (diluted and concentrated) are in equilibrium. This phase transition occurs for moderate volume fraction and $R_w = 2$ when the temperature is decreased. The temperature at which this second type of transition occurs for a given composition, depends on the molar mass and degree of branching of the oil (Table 1).

On the other hand, the conductivity of the solution increases as the temperature is decreased toward the phase separation temperature (Figure 5) and as either c (Figure 4) or R_w (Figure 3) increases. By small-angle scattering, a clear succession of shapes is observed when the same parameters are varied. The analysis clearly demonstrates that, along a water dilution line by increasing R_w at fixed c and T, the small globular aggregates formed at $R_w = 0$ undergo one-dimensional growth to give first rodlike micelles, and then, when these get sufficiently long, the longitudinal flexibility of the micelles become visible and wormlike micelles are observed (see Figures 6 and 7 and Table 2). The same succession of micellar shapes is observed if the concentration is increased for fixed R_w and T (see Table 2) or if the temperature is decreased for fixed R_w and c (see Figure 8 and Table 3). The development of the micelle shape from spherical to long and wormlike is also manifested in the results of the dynamic light scattering (Figure 9). Thus, the composition-induced growth of the micelles gives rise to respectively a strong increase of the conductivity (see Figures 3−5) and a concomitant increase growth of the hydrodynamic radius of the micelles (Figure 9).

Sphere-to-Wormlike Growth of the Micelles. As explained in section 4.4, a micellar growth, proportional to $c^{0.5}$, is predicted from a mean field theory. Such a growth behavior is for example experimentally observed in solutions of SDS in water.[34] For $R_w = 1$, we observe a concentration-induced micellar growth in good agreement with the mean field theory, whereas for $R_w = 2$, we observe a significantly stronger growth. The initial growth

(49) Cates, M.; Candau, S. *J. Phys.: Cond. Mater.* **1990**, *2*, 6869−6892.
(50) Schmidt, M.; Burchard, W. *Macromolecules* **1981**, *14*, 210−211.

of R_h is proportional to $c^{1.44}$ and therefore comparable to the so-called "enormous concentration-induced growth" reported by Schurtenberger et al for $C_{16}E_6$ micelles in water[51] where a growth rate of $c^{1.1}$ is reported and for inverse lecithin micelles in oil[52] where a growth rate of $c^{1.2}$ is reported.

Such growth has been explained in direct micelles by the ladder model of micellar growth.[53,54] The idea here is that as soon as the chemical potential of the surfactant, set in o/w micelles by the concentration of monomers in equilibrium with micelles, exceeds the curvature energy to change curved end caps into a section of a cylinder, unlimited growth can occur. In principle, the same mechanism can occur in indirect micelles and has been detailed in the form of shape dependent chemical potential by Israelachvili and Ninham.[55]

Polymorphism. The reverse microemulsion structure and phase behavior of the C8N8/water/octane system is extremely sensitive to the different experimental parameters studied. As explained above, the choice of surfactant concentration, c, water-to-surfactant ratio, R_w, and temperature, T, all have a strong influence on the microemulsion topology. The origin of polymorphism in self-assembled system is due to the minimization of the curvature energy given by

$$E = \int \left[\frac{1}{2}\kappa(c_1 + c_2 - c_0)^2 + \bar{\kappa}c_1c_2\right] \mathrm{d}a \qquad (13)$$

originally derived by Helfrich,[56] where c_0 is the spontaneous curvature, c_1 and c_2 are the two principal curvatures of the surfactant film, and where κ and $\bar{\kappa}$ are respectively the bending and saddle splay modulus. Steric constraints are also imposed by the composition of the solution, and the free energy can be rewritten using one bending constant only and taking into account the coverage relation.[57]

In the case of pure surfactant in oil (or water), at least one of the three dimensions of the object has to be smaller than twice the total length of the surfactant molecule to avoid holes in the hydrophilic (hydrophobic) part of the surfactant film.[58] In the case of microemulsions, the situation is different as the composition of the solution dictates conservation of the total volume and total surface of the aggregates. More precisely, the curvature of the surfactant film is imposed by the composition through the ratio between the volume of the inner phase and the total area of the surfactant film. The curvature energy depends on the product of the spontaneous curvature, c_0, and the actual radius of the water channels (which is proportional to R_w).[59]

The curvature energy will dictate the preferred shape that the micelles are likely to adopt depending mainly on c_0, R_w, and the thermodynamic properties of the surfactant film (the bending modulus κ and the saddle splay modulus $\bar{\kappa}$). As the water-to-surfactant ratio increases (at constant spontaneous curvature), the most stable topology is first lamellae and then a network of interconnected rods. When the inner phase content is further increased, the preferred topology will be disconnected rods and then spheres.[59,60]

In our system, we are starting by the neat catanionic/octane solutions where inverse spherical micelles are present. As the water-to-surfactant ratio increases, the micelles grow uniaxially into, first, short rodlike micelles, and then, long wormlike micelles appear.

In the biphasic system, the preferred micelle shape is spherical which shows that the spontaneous curvature is nonzero (at least higher than $(2l)^{-1}$ where l is the surfactant length), otherwise a dilute lamellar phase or a rodlike geometry would be preferred. The progressive transformation of sphere to cylinder upon addition of water is not the one which is predicted in a system where the dominant energetic contribution to the total energy is the elastic curvature energy. The explanation for this discrepancy could be that, for low values of R_w, the spontaneous curvature is certainly not constant. The first molecule of water is likely to bind strongly to the surfactant head and make the spontaneous curvature smaller. As the volume of the polar head is increased, the packing toward the oil phase will be favored.

At the emulsification failure, when thermal fluctuations can be neglected, the most stable phase is a phase of spheres. This is the overall most stable topology, and an increase of the water-to-surfactant ratio leads to an increase of the energy of the system. Rejection of the excess inner content and coexistence of water with a sphere of radius c_0^{-1} is thus the preferred configuration.[61]

In our system, at the emulsification failure, wormlike micelles are present in the equilibrium with pure water as stated in our study both by scattering techniques and by the conductivity. A microemulsion consisting of disconnected spheres would have a conductivity close to neat octane, whereas in our case, the conductivity at the emulsification failure is 2 orders of magnitude higher. Emulsification failures of cylinders and networks are predicted[62] when thermal fluctuations are included. When the spontaneous curvature approaches zero, the curvature-determined length scales increase and the saddle splay modulus may reach values close to zero (or even positive: $\bar{\kappa} \sim \ln(R/\xi)$ where $R \sim 1/c_0$ and ξ is the thermal persistence length.) Hence, the saddlelike shape of the junction will be stabilized toward spheres. This shows that in our system the spontaneous curvature is close to 0 at ambient temperature. The thermal fluctuation cannot be neglected in this case and renormalization of the saddle-splay modulus has to be taken into account. The influence of this parameter is rarely documented experimentally as it is difficult to relate it to the shape of the surfactant. In our case, as the length of the hydrocarbon chain is situated in the lower limit for surfactants, the bending moduli is certainly small[63,64] and thus the saddle splay modulus more important. These thermal fluctuations are also clearly visible in the scattering patterns as a model of semiflexible wormlike chains can properly fit the scattering patterns showing that the thermal fluctuation cannot be neglected.

Another experimental observation which may be explained by this simple model is the apparent reduction of the total length of the micelles for the concentrated samples as the water-to-surfactant ratio is increased above two. This is in agreement with the theoretical statement that a network of long wormlike chains will be transformed into rods and then spheres when the water-

(51) Schurtenberger, P.; Cavaco, C.; Tiberg, F.; Regev, O. *Langmuir* **1996**, *12*, 2894−2899.
(52) Schurtenberger, P.; Cavaco, C. *J. Phys. II France* **1994**, *4*, 305−317.
(53) Missel, P. J.; Mazer, N. A.; Benedek, G. B.; Young, C. Y.; Carey, M. C. *J. Phys. Chem.* **1980**, *84*, 1044−1057.
(54) Zoeller, N.; Lue, L.; Blankschtein, D. *Langmuir* **1997**, *13*, 5258−5275.
(55) Israelachvili, J. N.; Mitchell, D. J.; N. B. *J. Chem. Soc., Faraday Trans. 2* **1976**, *72*, 1525−1568.
(56) Helfrich, W. *Z. Naturforsch., C: J. Biosci.* **1973**, *28*, 693−703.
(57) Hyde, S.; Andersson, S.; Larsson, K.; Blum, Z.; Landh, T.; Lidin, S.; Ninham, B. *The Language of Shape*; Elsevier Science: New York, 1996.
(58) Porte, G. In *Micelles, membranes, microemulsions and monolayers*; Gelbart, W., Ben-Shaul, A., Roux, D., Eds.; Springer: New York, 1994; Chapter 2, pp 105−151.
(59) Safran, S.; Turkevich, L.; Pincus, P. *J. Phys. Lett. (Paris)* **1984**, *45*, 19.
(60) Ninham, B.; Barne, I.; Hyde, S.; Derian, P.; T. N., Z. *Eur. Phys. Lett.* **1987**, *4*, 561−568.
(61) Safran, S.; Turkevich, L. *Phys. Rev. Lett.* **1983**, *50*, 1930−1933.
(62) Tlusty, T.; Safran, S. *Science* **2000**, *290*, 1328−1331.
(63) Rekvig, L.; Hafskjold, B.; Smit, B. *Phys. Rev. Lett.* **2004**, *92*, 116101.
(64) Szleifer, I.; Kramer, D.; Ben-Shaul, A.; Gelbart, W.; Safran, S. *J. Chem. Phys.* **1990**, *92*, 6800−6817.

to-surfactant ratio is increased.[59] However, we do not observe the rod to sphere transition as emulsification failure occurs before.

Temperature Dependence of the Curvature. A temperature dependence of the spontaneous curvature of the C8N8 is directly manifested in the strong temperature induced micellar growth documented in Figure 8 and Table 3. As the water-to-surfactant ratio is constant, the change in topology can be explained by a change in the spontaneous curvature of the surfactant film. As the temperature decreases, the spontaneous curvature (positive toward water) decreases, and hence, long flexible micelles are preferred as rounded end-caps which have locally important curvature toward water are destabilized. This assertion is also confirmed by the temperature dependence of the emulsification failure boundary. At a low temperature, the microemulsion can solubilize more water than at a high temperature as shown in Figure 1. Hence, the spontaneous curvature decreases when the temperature is decreased.

The temperature dependence of the spontaneous curvature is also shown by the liquid−gas-phase separation. In the L_2 phase, when the temperature is further decreased, at a certain point, a phase separation occurs and leads to two microemulsions in equilibrium. This kind of phase separation has already been observed in solutions of wormlike micelles.[65,66] In every case, it occurs after a huge increase of the apparent length of the wormlike micelles induced by the variation of a triggering parameter (addition of water in the case of a lecithin-based microemulsion,[65] addition of bile salt in lecithin, bile salt mixtures[66]).

The physical origin of this phase separation can be discussed. A nematic/isotropic[67] phase transition which would be possible in our case as we are dealing with anisotropic objects is unlikely here as the concentrated microemulsion does not show birefringeance. A liquid−gas transition is likely to occur as the connection points between wormlike micelles act as an effective attraction, more effective than van der Waals forces only. When the temperature is decreased, the spontaneous curvature decreases, and junctions are more numerous. Since the concentrated solutions remain fluid (a direct proof of the existence of branching more frequent than entanglement) and present high conductivities (a proof of connectivity of the water domains on a macroscopic scale), the mechanism must be an entropic phase separation induced by the multiplication of branched points linking the wormlike chains.

The re-entrant phase separation is predicted by the theory of Tlusty, Safran, and co-workers[48,62,68] by considering an equilibrium between junctions and free ends in dipolar fluids.

The presence of a microemulsion structure consisting of a connected network of long cylinders has been demonstrated since a long time to explain several features of ionic microemulsion systems, including the broad peak in the scattering patterns and the antipercolation phenomenon which are both included in the DOC model of microemulsions.[69−71]

In the Tlusty−Safran theory,[48,72,73] the structure of the microemulsion has to be considered at two different length scales. The local length scale is governed by the bending elasticity of the surfactant film (see the previous paragraph). If a cylindrical local structure is preferred thermodynamically, then, on larger length scales, the organization of the cylinders is governed by thermal fluctuations through the interplay between end-caps and junctions. This balance is strongly temperature-dependent through the dependence of the spontaneous curvature. Junctions are favored by small curvature due to their lamellar core while end-caps by high curvature. Junctions act as an effective attraction and when they are too numerous, yield to a phase separation triggered by an effective attraction. On a molecular level, the driving force of this temperature dependence of the C8N8 film is most likely similar to the one observed for alkyl polyglycol ether surfactants where the hydration of the polar head is strongly temperature dependent.[74] As the temperature increases, less hydration water is bound to the surfactant head for entropic reasons. Hence, the surface area per polar head is reduced, and the surfactant becomes more strongly curved toward water as temperature increases. A strong penetration of the oil chain in the surfactant tail will increase the spontaneous curvature as the packing will be favorable to structures curved toward water. Hence, to make junctions, which are likely at small spontaneous curvature, the temperature of the $L_2 + L_2$ demixion will have to be smaller in the case of penetrating oils. This is experimentally observed as reported in Table 1. For hexane, a very penetrating oil, the demixion occurs at 6 °C. This temperature is increased when the length of the oil chain is increased which makes the penetration of the oil less likely.

Signs of Micellar Branching in the Experimental Data? The predictions of the Tlusty−Safran theory suggest performing a second investigation of our experimental data with the special aim of searching for direct or indirect signs of branched structures.

As mentioned in section 3.2, from a stuctural point of view, a branching of the wormlike micelles should give rise to a power-law behavior with an exponent higher than the 5/3 we obtain from regular wormlike chains. The samples that should contain the most clearly visible signs of such a behavior would be samples measured near the liquid−gaslike phase separation and at sufficiently low concentrations so that information about the power-law is not drowned by the intermicelle structure factor. No indications of a more steep power-law behavior from a branched structure is observed in any of the data. Instead the $q^{-5/3}$ behavior extends down to very low q values in several of the data set. In particular, in the sample measured at $T = 23$ °C (Figure 8), i.e., right before the lower, liquid−gaslike, phase transition, we observe that the $q^{-5/3}$ behavior extends all of the way down to $q \sim 0.003$ Å^{-1}. Thus, on a length scale corresponding to $D = 2\pi/q = 2000$ Å, the micelles have a locally wormlike structure and branching effects are nonsignificant in the SANS data.

An increased attraction between the micelles is anticipated when the temperature is decreased toward the lower phase separation temperature and could be related to an increased number of junction points. However, the SANS data from the temperature scan (Figure 8) do not contain an unambiguous proof of increased attraction between the micelles. Again, the effects of attraction should be most clearly visible at the lowermost temperature, $T = 23$ °C. But as is seen, the data measured at this temperature agree perfectly with the $q^{-5/3}$ behavior compatible with poorly or disconnected wormlike micelles. Instead, the attraction shows up indirectly in the interparticle interactions where it gives rise to an apparent lowering of the excluded volume effects in such a way that the structure factor apparently becomes

(65) Shchipunov, Y. A.; Hoffmann, H. *Langmuir* **1998**, *14*, 6350−6360.
(66) Tung, S.; Huang, Y.; Raghavan, S. *J. Am. Chem. Soc.* **2006**, *128* (17), 5751−5765.
(67) Onsager, L. *Ann. N.Y. Acad. Sci.* **1949**, *51*, 627−659.
(68) Zilman, A.; Tlusty, T.; Safran, S. *J. Phys.: Cond. Mater.* **2003**, *15*, S57−S64.
(69) Zemb, T.; Hyde, P.; Barnes, I.; Ninham, B. *J. Phys. Chem.* **1987**, *91*, 3814.
(70) Barnes, I.; Hyde, S.; Ninham, B.; Derian, P.; Drifford, M.; Zemb, T. *J. Phys. Chem.* **1988**, *92*, 2286−2293.
(71) Zemb, T. *Colloids Surf. A* **1997**, *129−130*, 435−454.
(72) Tlusty, T.; Safran, S.; Menes, R.; Strey, R. *Phys. Rev. Lett.* **1997**, *78*, 2616−2619.
(73) Tlusty, T.; Safran, S. *J. Phys.: Cond. Mater.* **2000**, *12*, A253−A262.
(74) Strey, R. *Colloid Polym. Sci.* **1994**, *272* (8), 1005−1019.

vanishing as the lower phase boundary temperature is approached. This indicates that attractive interactions are present but have not yet become dominant at this temperature and/or on the probed experimental length scales. However, the fact that the $q^{-5/3}$ behavior extends all of the way down to the minimal accessible q value of the $T = 23$ °C data and that no effects of the structure factor are observed indicate that the inter-micellar excluded volume effects have become partly counter-balanced by attraction effects, as the lower phase boundary temperature is approached.

The most direct sign of junction cannot be found in the scattering pattern. When connections become present, the macroscopic conductivity of the samples should increase strongly. Figure 9 shows the variation of the normalized conductivity versus the surfactant concentration for $R_w = 2$. The steep increase of the conductivity from $c = 0.4$ M suggests that a water network is forming in the octane solution when the surfactant concentration is sufficiently high. The conductivity is also strongly depending on the temperature as can be seen in Figure 9. As the temperature is decreased and approaches the lower phase separation temperature, the conductivity increases, which again suggests the formation of a more and more connected network when the phase separation is approached.

Wormlike micelles have previously been observed in the ternary system alkane/lecithin/water.[19,20,51] In cyclohexane and isooctane, the wormlike micellar structure appears as a highly viscous gel often termed as an organogel. In our case, the reverse microemulsion C8N8/water/octane has an apparent small viscoelasticity and no gel is observed along the water dilution lines. Since a connected network of branched micelles will have a lower viscosity than an entangled network of linear micelles,[25,75] this observation speaks in favor of the presence of junctions rather than entanglements.

(75) Lequeux, F. *Europhys. Lett.* **1992**, *19*, 675.

Thus, the Tlusty-Safran theory, as an extension of the DOC-model taking into account an effective attraction each time a connection point between connected cylinder appears, rationalizes the general phase behavior of the C8N8/water/octane system. Moreover, the conductivity data and the rheological behavior of our samples are in excellent agreement with their picture of a branched tubular microstructure even if the scattering data do not provide us any unambiguous proof of this structure.

6. Conclusion

At equimolarity, the surfactant film of the catanionic microemulsion system composed by alkylammonium octanoate, alkane, and water is not charged. When no water is present in the system, small reverse spherical micelles are formed. When the water-to-surfactant ratio, R_w, is raised to one or two water molecules per surfactant, the shape of the micelles is transformed into short cylindrically shaped micelles. If even more water is added, the micelles exhibit a very strong one-dimensional growth and are more appropriately described as long wormlike micelles. A likewise strong, one-dimensional growth is observed if the overall surfactant concentration is increased for fixed R_w or if temperature is decreased toward the lower phase boundary of the one-phase system. The curvature of the surfactant film decreases when temperature is decreased toward the lower phase boundary as in typical nonionic surfactants, such as C*i*E*j*. Changing the relative stoichiometry of the pair of ionic surfactant used and hence charging the interface should impact the parameters which dictates the physics of this system, this will be the subject of a forthcoming article.

Acknowledgment. We thank Julie Goyon for experimental help; Grégoire Porte, Michel Delsanti, and Luc Belloni for fruitful discussions, and the Institut Laue-Langevin for provision of the beam-time.

LA061465R